ACES Asian Chemical Editorial Society

DOI: 10.1002/cnma.201700371

CHEMNANOMAT
Full Paper

Cluster Crystals

Probing the Mechanical Response of Luminescent Dithiol-Protected $Ag_{29}(BDT)_{12}(TPP)_4$ Cluster Crystals

Korath Shivan Sugi,[a] Gangapuram Mallikarjunachari,[b] Anirban Som,[a] Pijush Ghosh,*[b] and Thalappil Pradeep*[a]

Abstract: Atomically precise clusters of noble metals are considered to be an important class of advanced materials. Crystals of these clusters composed of inorganic cores and organic ligands are fascinating owing to their tunable and unique properties. Understanding their mechanical properties can give more insight into the design of nanocluster-based devices. Here, we probe the mechanical response of single crystals of $Ag_{29}(BDT)_{12}(TPP)_4$ cluster (BDT = 1,3 benzenedithiol, TPP = triphenylphosphine) under both quasi-static and dynamic loading conditions. Surprisingly, the measured reduced Young's modulus (E_r) and hardness (H) were 4.48 and 0.285 GPa, respectively, similar to those of polymers and much smaller than the values for bulk silver. These observations indicate a significant role of capping ligands on the physical properties of such materials. The observed storage modulus, loss modulus and loss factor were also found to be similar to those of polymers. The magnitude of loss factor suggested the ability of nanocrystals to absorb energy under dynamic loading. These studies of mechanical properties of cluster materials could be useful in developing their applications.

Introduction

Atomically precise nanometer-sized pieces of noble metals, protected with ligands having well-defined crystal structures[1] belong to a new category of materials. They are distinctly different from nanoparticles in their spectroscopic properties, such as well-defined features in their optical absorption and emission spectra, just like molecules, which has been efficiently manipulated to create functional devices. Luminescent properties of these noble metal nanoclusters (NMNCs) have been used in the creation of sensors.[2] In contrast, nanoparticles of such metals composed of thousands of atoms exhibit strong surface plasmon resonance and nearly undetectable luminescence. Due to their pronounced luminescence, NMNCs are successfully conjugated with other functional materials for the creation of solar cells.[3] They are also used as cocatalysts in improving the performance of MoS_2 towards hydrogen evolution reaction (HER).[4] Such exciting optical, electronic properties of these materials can be enhanced further by changing the size and shape of the metal core during synthesis or by alloying.[5]

These NMNCs, synthesized in solution, make crystals under controlled conditions. Total structures of many of these clusters have been solved by growing such single crystals. Kornberg group in 2007 reported the first crystal structure of the decahedral Au_{102}.[1d] Total structures of several other gold clusters like Au_{18},[6] Au_{20},[7] Au_{23},[8] Au_{24},[9] Au_{25},[10] Au_{28},[11] Au_{30},[12] Au_{36},[13] Au_{38}[14] and Au_{133}[15] of varying crystal systems have been reported till date. In the case of silver clusters, although the developments have been slower, some reports have become available in recent years which include Ag_{14},[16] Ag_{25},[17] Ag_{29},[18] Ag_{44}[1e] and Ag_{67}.[19] All the clusters are protected with ligands, often thiolates and have counter ion to compensate charges. For example, Ag_{44} exists as $[Ag_{44}(SR)_{30}]^{4-}Na_4$. Functional groups present on the organic ligands of these NMNCs interact chemically between neighboring NMNCs and dictate the orientation and packing of the nanocluster (NC) in the crystal.[20] Controlling such ligand-ligand interactions open up possibilities to further tune and optimize the properties of NMNCs for applications in optical and electronic devices. In the recent past, physical properties such as hardness (H) and Young's modulus (E_r) have been correlated well with molecular properties.[21] Interesting observations have been made in the context of solubility and mechanical properties of pharmaceuticals which are relevant in the context of drug delivery.[22] Due to the presence of long-range order in the NC crystals, it is likely that physical properties of such crystals will be closely related to the molecular structure of the individual NC, much like fullerenes.[23]

Nanoindentation[24] is a reliable method to precisely understand bulk mechanical properties of materials. Recently, the nanoindentation technique has been widely used for evaluating the mechanical properties of various organic and inorganic

[a] K. S. Sugi, A. Som, Prof. T. Pradeep
DST Unit of Nanoscience (DST UNS) and Thematic Unit of Excellence (TUE), Department of Chemistry, Indian Institute of Technology Madras, Chennai 600 036, India
E-mail: pradeep@iitm.ac.in
[b] G. Mallikarjunachari, Prof. P. Ghosh
Department of Applied Mechanics & Soft Matter Center, Indian Institute of Technology Madras, Chennai 600 036, India
E-mail: pijush@iitm.ac.in

Supporting information for this article is available on the WWW under https://doi.org/10.1002/cnma.201700371

crystals as well as metal-organic frameworks (MOFs).[25] Such studies indicate an important correlation between mechanical and molecular aspects of materials. Assembly of plasmonic metal or semiconductor nanoparticles, forming superlattice crystals, has been a subject of study.[26] Electronic properties of such materials from the context of origin of metallicity has been examined in detail.[26a] Nanocrystal superlattices exhibit superior mechanical strength and are capable of withstanding repeated indents.[26b,27] Such remarkable mechanical cohesion in the superlattices are due to the van der Waals interactions between ligands on neighboring nanocrystals.[28] Due to versatile properties of Au nanocrystals, considerable effort has been paid to understand their mechanical properties. Mueggenburg et al. had reported that the dodecanethiol-ligated gold nanocrystal monolayers, have Young's modulus of the order of several GPa and they remain intact and able to withstand tensile stresses up to temperatures around 370 K.[26b] Nanoindentation studies performed on oleic acid stabilized PbS nanoparticles by Tam et al. attributed the mechanical properties to the organic capping agents surrounding the inorganic core.[29] Similar studies by Podsiadlo et al. on both the shaped superlattice crystals and the evaporated, layer-by-layer superlattice crystals correlated the mechanical properties of PbS, CdSe, and $CoPt_3$ superlattice crystals with the nanocrystal size, capping ligands, and degree of ordering.[26c]

Single crystals of NMNCs are different from all these materials as in former case atomically precise NCs are assembled into macroscopically ordered crystals. While the optical and electronic properties of NMNCs are being intensely researched upon, mechanical properties of such materials are yet to receive significant attention. However, properties of NMNC-based devices would depend also on their mechanical properties (like hardness and modulus, etc.), which emphasizes the need to study and understand them in detail. Moreover, all of these properties of a NMNC-crystal will depend upon how strongly a NMNC interacts with its neighboring clusters. While such interactions are difficult to study experimentally at single NMNC level, bulk mechanical properties can be correlated to NC-NC interactions in the crystal.

Herein, we present an early investigation into the mechanical properties of one such silver NC system. The present study focuses on mechanical properties of crystals of bidentate thiol protected, highly stable[30] $Ag_{29}(BDT)_{12}(TPP)_4$ NCs (BDT – 1,3 benzenedithiol, TPP – triphenylphosphine), for which the light-harvesting capabilities and charge transfer dynamics[31] were well studied recently. The cluster crystal is referred to as **I** in the following discussion. This makes such systems promising candidates for NC-based devices. Nanomechanical characterization techniques, such as nanoindentation, nanoscratch, and nano-dynamic mechanical analysis (DMA) have been applied to understand the mechanical properties of **I**. Quasi-static nanoindentation was applied to determine the two fundamental properties, E_r and H of the **I**. The storage modulus, loss modulus and loss factor at different frequencies were determined by applying dynamic loading. Nanoscratch technique was applied to examine the material heterogeneity, if any, along and across the depth. We find that the E_r and H of **I** are 4.48 and 0.285 GPa, respectively, far lower than the respective values of bulk silver (62.52 and 3.57 GPa). Interestingly, these properties are similar to commonly known polymers such as polymethyl methacrylate (PMMA). The clusters were found to be intact under experimental investigations and no change in electronic properties was observed.

Results and Discussion

ESI MS was employed to confirm the composition and purity of the $Ag_{29}(BDT)_{12}(TPP)_4$ cluster. The negative ion mode mass spectrum of the purified cluster is shown in Figure 1a which

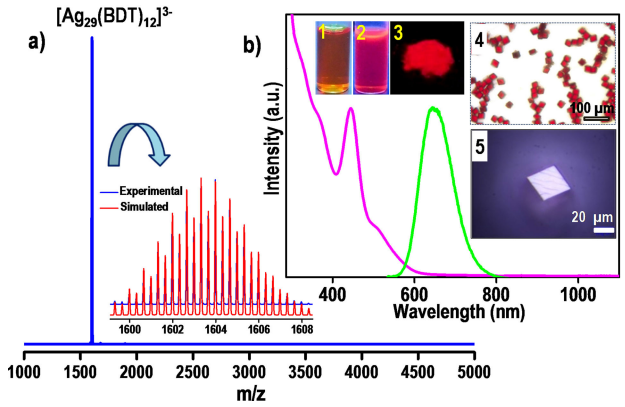

Figure 1. a) Negative ion mode SI-MS of $Ag_{29}(BDT)_{12}(TPP)_4$ clusters. The inset shows the comparison of experimental and simulated mass spectra of $[Ag_{29}(BDT)_{12}]^{3-}$ which match exactly. b) Optical absorption (pink) and emission spectra (green) of $Ag_{29}(BDT)_{12}(TPP)_4$ clusters. The excitation wavelength is 450 nm. Inset 1 and 2 are the photographs of the cluster solution under visible and UV light, respectively. Inset 3 is the photograph of the cluster powder under UV light. Inset 4 and 5 are the optical images of **I** collected in transmission and reflected modes, respectively.

agrees well with the reported spectrum of $Ag_{29}(BDT)_{12}(TPP)_4$. The peak centered at 1603 corresponds to $[Ag_{29}(BDT)_{12}]^{3-}$ as the weakly bonded phosphines dissociate during ionization. Expansion of the peak centered at 1603 shows a characteristic isotropic distribution in which each peak separation corresponds to $m/z = 0.33$, which in turn corresponds to the -3 charge state. The optical characterization of clusters was done using UV-vis and photoluminescence (PL) measurements. Figure 1b shows the UV-vis absorption spectrum (pink trace) and emission spectrum (green trace) of the $Ag_{29}(BDT)_{12}(TPP)_4$ cluster solutions. Molecular transitions are observed at 447 and 513 nm. When excited at 450 nm, the emission maximum was observed around 670 nm. Inset 1 of Figure 1b is the photograph of cluster solution in visible light and inset 2 is the photograph under UV light. Inset 3 is the photograph of the cluster powder under UV light. The purified cluster was crystallized in a dark box for a period of 3–4 days. After four days, red square plate-shaped crystals were observed. Insets 4 and 5 of Figure 1b are the optical images of the **I** collected in the transmission and reflected modes, respectively. The cluster crystallizes in cubic Pa3 space group. The crystal structure of

the cluster is shown in Figure S1a (Supporting Information). The SEM image of the cluster crystals also confirms the formation of uniform cubical crystals (Figure S2).

Compared to other mechanical investigations, nanoindentation leaves only a small imprint on materials and can be considered as a non-destructive technique even though sharp indenters are used to penetrate the surface of the sample. A typical load-displacement curve during loading and unloading is shown in Figure S3. The label, h_{max} is the maximum penetration depth associated with the applied maximum load P_{max}; h_p is the residual penetration depth at full unloading while h_e is the elastic penetration depth recovered at full unloading and h_c is the contact depth under the maximum indentation force. In our experiments with **I**, a holding time of 10 s before unloading was applied to reduce the effect of creep on the measured quantities. An optical microscope was used to position the indenter tip over nanocrystals. The E_r and H were determined from load-displacement curves by applying Oliver and Pharr analysis.[32] The Oliver–Pharr method is the most common method used for establishing the projected contact area and predicting the elastic modulus of ordinary materials. In this method, the unloading portion of indentation graph was fitted into the power-law,

$$P = B(h - hp)^m \quad (1)$$

where, B and m are fitting parameters and h_p is the final indentation depth after complete unloading.

According to this method, in the absence of creep, the initial unloading of the sample is elastic and the contact area stays constant. Stiffness (S) is the measure of the resistance offered by an elastic body to deformation. The slope of initial part of the unloading curve thus represents the stiffness of the indented material. From this data, the initial unloading slope, i.e., contact stiffness S is estimated by analytically differentiating Equation (1) and evaluating the result at the maximum indentation depth.

$$S = \left(\frac{dP}{dh}\right)_{h-h_{max}} = Bm(h_{max} - h_p)^{m-1} \quad (2)$$

where, P is the applied load and h is the displacement. Finally, in the case of a rigid indenter, the elastic modulus E_r is calculated by

$$E_r = \frac{1}{\beta}\frac{\sqrt{\pi}}{2}\frac{S}{\sqrt{A}} \quad (3)$$

where, β is the correction factor.

The hardness of a material is the measure of its ability to resist plastic deformation and is given by the Equation (4).

$$H = \frac{P_{max}}{A} \quad (4)$$

where, P_{max} is the peak indentation load and A is the projected area of the impression. The nanocrystals are crystallized on a glass microscope slide. To avoid the substrate effect, all the experiments were performed such that the maximum depth of penetration attained remained below 10% of the crystal size. We performed load dependent studies initially on **I** (Figure S4) by applying a series of loads, such as 50 μN, 100 μN, 150 μN and 200 μN and corresponding moduli were determined. The E_r depends mainly on S and the A of the residual imprint. As peak load increases, these two factors changes, thus affecting the Young's modulus. The variation of E_r and H with increasing load is shown in Figure S5. The modulus and hardness values corresponding to lower loads were disregarded since those represent more of the surface properties and not of the bulk. Also, due to low displacement in the normal directions at lower loads, the surface roughness influences the response of the true material. The load-displacement response of a single crystal at 200 μN is shown in Figure 2. The schematic of

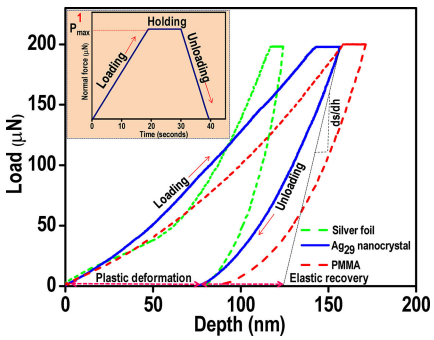

Figure 2. Load-displacement curves of silver foil (green dotted line), **I** (blue solid line) and PMMA (red dotted line) with Berkovich indenter. Inset 1 shows a schematic of the trapezoidal load function.

trapezoidal load function used for indentation is shown in the inset of Figure 2. The loading part of the curve is elastic-plastic in nature. The slope of the initial part of the unloading curve represents the elastic recovery of the material and thus is applied to estimate the elastic modulus of a material. For comparison, NI tests were also performed on a silver foil and PMMA. The values determined at 200 μN load are shown in Table 1. The E_r and H values corresponding to 200 μN can be considered as representative bulk values. These E_r and H values obtained for **I** were 4.48 (±0.115) GPa and 0.285 (±0.006 GPa), respectively.

It is to be noted that the elastic modulus of **I** is similar to that of some of the widely-used polymers such as PMMA and polystyrene[33] and is significantly different from silver metal, which constitutes the cluster core. The large Young's modulus in polymers is attributed to the entanglement of monomer

Table 1. Measured Young's modulus and hardness of the different materials

Material	E_r (Gpa)	H (Gpa)
Silver foil	62.52 ± 1.8	3.57 ± 0.250
Ag_{29} nanocrystal	4.48 ± 0.115	0.285 ± 0.006
PMMA	3.90 ± 0.155	0.187 ± 0.030

molecules.[34] In case of **I** the Young's modulus is presumably a consequence of the ligand confinement and associated interactions. This observation suggested that the protecting ligands not only act as spacers but also provide significant mechanical strength through ligand-ligand interactions.

The initial part of the unloading curve of the load-displacement plot indicates elastic recovery (Figure 2). The area under the respective elastic recovery region and plastic deformation region of load-displacement curve provides an insight into the elastic work done (W_E) and the energy dissipated (W_P) due to plastic deformation during the application of load (Figure S6). W_E is the amount of energy utilized in deforming a material which recovers when the load is removed and plastic work done W_P is the amount of energy dissipated while the material undergoes plastic deformation. The calculated ratio of W_P to W_E from the load-displacement curve of the crystal is 1.89 which further confirms the permanent deformation in the crystal. The permanent deformation in the nanocrystal possibly arises from the relative displacement of the clusters under the applied load.

It is observed from the load-displacement plot that during the hold time of 10 s, the crystal underwent a creep displacement of about 14 ± 2 nm. Creep[35] is a phenomenon where under a constant load; a visco-elastic material undergoes displacement. Under identical conditions, PMMA showed a comparable creep displacement of 12 ± 2 nm. The presence of organic ligands, therefore, contributes to the time-dependent creep behavior of **I**.

The residual indentation impression of the indented surface of the nanocrystal is shown in Figure 3a. In the normal direction, the maximum depth of penetration of 170 nm was attained under the maximum load; whereas with the removal of the load, the nanocrystal recovered, leaving a residual depth of 40 nm. The number of unit cells subjected to direct load under the indenter was calculated by measuring the volume of residual impression from the piezo image. The volume of indentation imprint is 3.181×10^{-21} m^3. The volume of the molecular crystal unit cell is 40006×10^{-30} m^3. Therefore, the number of unit cells subjected to direct load under the indenter is approximately 7.952×10^4. This translates to a number of 6.362×10^5 clusters under the indented volume. These are also approximately the number of clusters which have undergone permanent deformation and thus contribute to the plastic energy (W_p). The variation observed in the values of H for PMMA and the nanocrystal (Table 1) is due to the difference in maximum displacement (Figure 2). This is because the area of residual indentation imprint used for calculating hardness changes with the change in maximum displacement. The slightly higher value of hardness of the nanocrystal could be due to the even distribution of stress in **I** than a polymer network.

To investigate the strength of **I**, we have performed indentation with a higher load of 10000 μN (Figure S7a). There was no evidence of fracture even at such high loads (Figure S7b and c). The indentation was also performed at higher loading rate, i.e., 10000 μN/s; however, still no fracture or crack propagation was observed in the SEM image of the residual indentation imprint (Figure S7d and e). The absence of any formation or propagation of cracks even at higher loads might be due to the ligand-ligand interactions in the nanocrystal which imparts such ductile (visco-elastic) nature to the material.

Pile-up is a phenomenon of accumulation of materials on the surface around the indenter tip resulting in plastic deformation due to the applied load. Since the elastic modulus of **I** is similar to that of PMMA and also the fact that it exhibits creep behavior, we have measured the pile-up of **I** during indentation. The section profiles of the nanocrystal and PMMA (Figure 3b) were taken along the indentation impression (dotted red line) as shown Figure 3a. The PMMA exhibits slight pile-up whereas no pile-up was observed in the case of **I** which might be due to its work hardening capacity. Work hardening in materials is induced normally when the density of disloca-

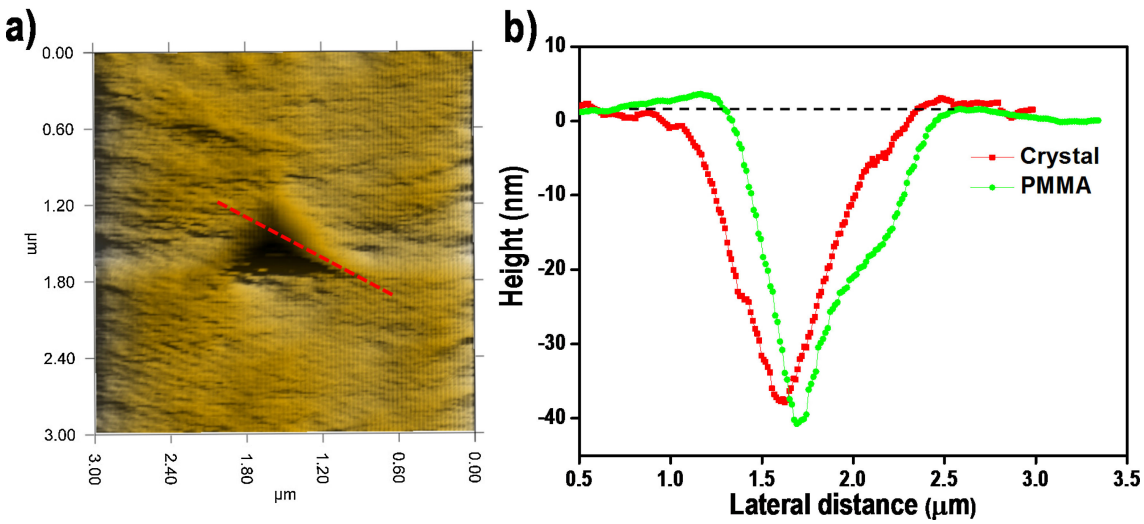

Figure 3. a) Piezo image of residual indentation imprint on **I**. b) Cross-sectional profile of the indentation imprint in **I** along with the dotted line (in red), is shown in comparison with that of PMMA (in green).

tions becomes sufficient that they begin to interact and hamper further deformation.[36] In general, the pile-up is greatest in materials with large E_r/H and thereby such systems will not have much work hardening capacity. The capacity for work hardening inhibits the pile-up because the hardening of material during deformation at the proximity of indenter tip constrains the upward flow of material to the surface. The value of E_r/H obtained for **I** was 15.71 and that of PMMA was 20.85, respectively. In case of **I**, the volume of material under the indenter tip could possibly be experiencing significant compaction thus preventing any pile-up. Under applied stress, the benzene rings in the cluster might have oriented by tipping of the planes in the direction of the load. This could result in the interdigitation of ligands in the proximity of the indenter (Figure S8).

In order to confirm that the electronic structure of the cluster remains intact before and after indentation, emission spectra were collected from the indentation spot before and after nanoindentation with a confocal Raman microscope. The emission spectra (Figure 4) remain essentially the same before and after indentation confirming the stability of the clusters. The observed shift in the spectra before and after indentation was found to be 6 nm. However, spectral shifts in nanoclusters due to structural changes are found to be significantly higher, to the extent of hundreds of nm. Therefore, we concluded that the nanoindentation did not affect the overall structures of the nanoclusters. The observed small shift in the spectra might stem from the slight reorientation of the ligands due to compaction caused by nanoindentation. Inset 1 and 2 of Figure 4 are the optical images of the nanocrystals before and after indentation.

Since the E_r, H and creep behavior of the nanocrystals strongly resembled that of a polymer, DMA was performed to understand the frequency sensitivity of different polymeric properties, particularly the loss and storage modulus. The storage modulus (in-phase component) is an indication of the amount of energy restored as the dynamic load is removed, whereas, the loss modulus (out-of-phase component) is a measure of energy dissipated or lost in undergoing permanent changes. The storage modulus is the dynamic counterpart of elastic modulus. The ratio of loss to storage modulus of a material is quantified as tan δ, also known as damping or loss

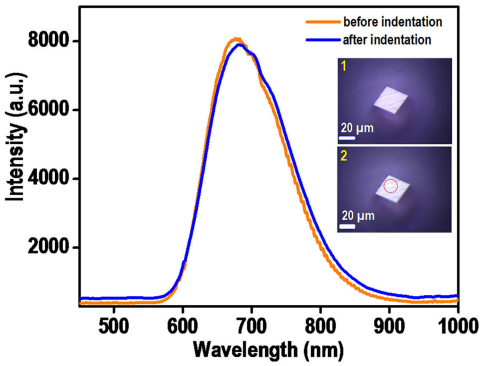

Figure 4. Emission spectra of **I** before and after indentation collected from the indentation spot (red dotted circle). Insets 1 and 2 are the optical images of **I** before and after indentation.

factor. This factor indicates the ability of a material to absorb energy through different internal mechanisms when subjected to dynamic loading. The tan δ values of 0° and 90° represent a purely elastic and viscous material, respectively. Sinusoidal (AC) load of 10 μN was applied over a frequency range of 10 to 200 Hz. Assuming linear viscoelasticity, the frequency dependent dynamic response of the material can be determined using the following Equation 5 and 6, respectively.

$$E'(storage) = \frac{K_s\sqrt{\pi}}{2\sqrt{A_c}} \quad (5)$$

$$\tan\delta = \frac{\omega C_s}{K_s} \quad (6)$$

where, E' is the storage modulus and ω is the frequency of the applied load and K_S and C_S are the sample stiffness and damping coefficients, respectively and A_C is the projected contact area of the indent on the surface of the specimen.

The variation of storage modulus with frequency for the **I** is shown in Figure 5a. The dynamic response of PMMA is also depicted in Figure 5a for comparison after necessary corrections. The nanocrystal shows increase in storage modulus at higher frequencies similar to that of a polymer. At higher frequencies, polymer network does not get sufficient time to

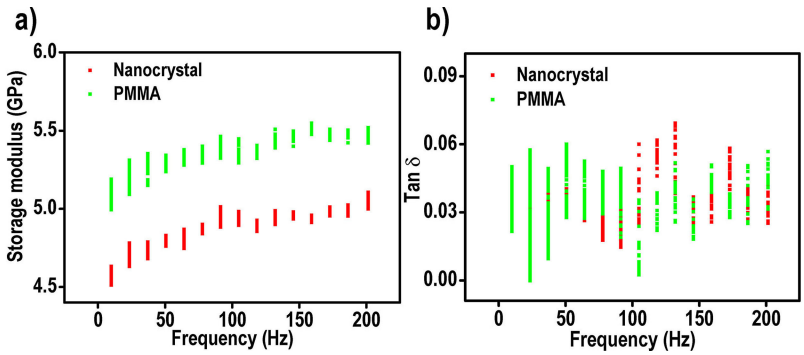

Figure 5. a) Variation of storage modulus with frequency for **I** (red) and PMMA (green). b) Variation of tan δ with frequency for **I** (red) and PMMA (green).

undergo the necessary relaxation and thus behave more like a stiffened mass, showing higher modulus. The storage modulus value for the nanocrystal ranges from 4.5 GPa to 5.5 GPa in the frequency range of 10 Hz to 200 Hz. Also, the value of storage modulus determined is in the range of the elastic modulus measured in quasi-static indentation test. The loss modulus varies from 0.1 to 0.3 GPa in the same frequency range (Figure S9). The variation of tan δ with frequency is shown in Figure 5b.

Any significant difference in the value of tan δ was not observed with the change in frequency. The magnitude of loss modulus and tan δ obtained for the nanocrystal indicates that it has the ability to absorb some energy under dynamic loading. Interdigitation of ligands and segmental motions of the clusters together could help in the energy dissipation in the nanocrystal. The characteristic tan δ of **I** is also very similar to that of PMMA (Figure 5b). However, the observed tan δ value is not as high as shock absorbing polymeric foams, where it's in the range of 0.6 to 0.7 at room temperature.[37]

Nanoscratch technique was applied to examine the homogeneity across the depth of **I**. In nanoscratch experiment, the indenter with constant load is glided through the surface of the nanocrystal. The lateral force experienced during scratching was recorded as a function of lateral displacement. Schematic representation of the nanoscratch technique is demonstrated in Figure 6a. Different sets of normal loads, 100 μN, 200 μN and 300 μN were applied separately on three different crystals. Scratch length of 5 μm was made with different penetration depths. The piezo images of the scratch made with 300 μN load and a penetration depth of 250 nm are shown in Figure 6b and 6c. The rumpled structures observed at the end of the scratch is rear pile-up formed by the aggregation of wear debris. The lateral force-displacement plots (Figure 6d) reveal the slight uneven force experienced by the indenter tip which presumably is due to the steps or undulations present on the surface of **I**. The friction coefficient plots with different scratch depth are shown in Figure 6e. The coefficient of friction along the lateral length is calculated from the nanoscratch experiments. It is defined as the ratio of the lateral load over the normal load. The variations observed in the friction coefficient plots (Figure 6e) might be due to the steps or undulations in **I**. During nanoscratch, i.e. when the tip slides over the crystal surface, a sudden change in lateral load is expected due to the presence of the steps which may be resulted in the variation of the friction coefficient. Cluster crystals, being grown in solution may incorporate solvent molecules. There is a possibility that these molecules may be lost upon storage. While this may not change the electronic properties such as luminescence of the crystal as well as structural features, the appearance of the crystal may be affected. In view of these, we have measured the mechanical properties of as prepared and aged **I** which do not show much difference in the E_r value (Figure S10). The dimensions of the indenter are much below the separation between the surface defects and therefore the indenter probes a defect-free region, as has been noted earlier in case of PbS nanocrystals.[26c] Both the fresh and aged crystals have same unit cell parameters as that of cubic **I**. Also, the variation in the friction coefficient was observed mainly at lower depths but was not much prominent at a depth of 250 nm. This observation confirms that the steps or undulations are present

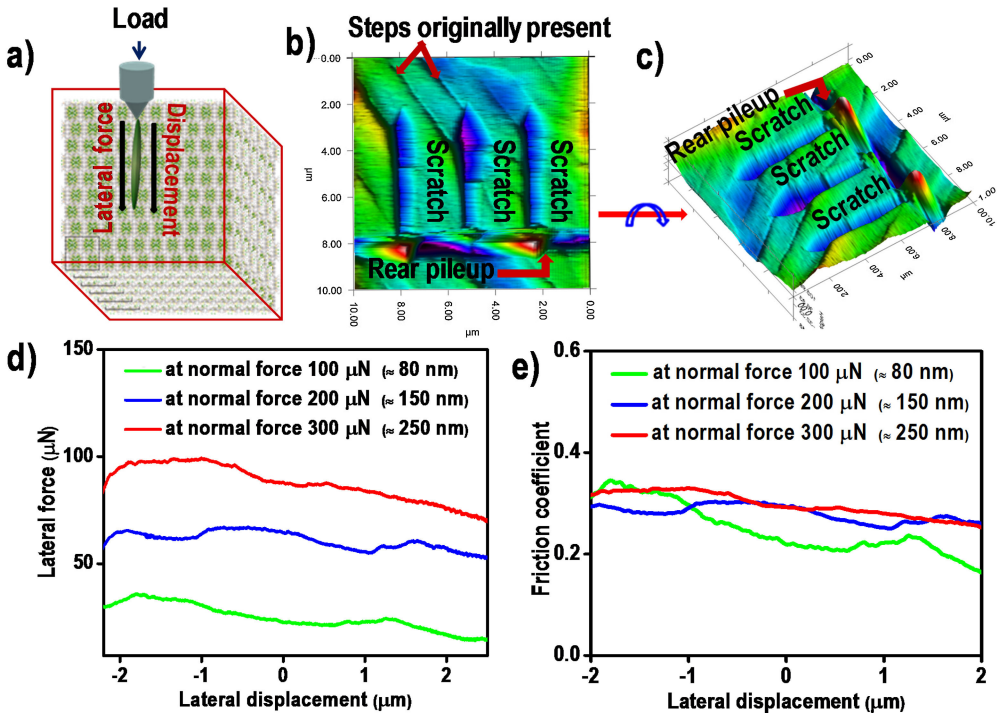

Figure 6. a) Schematic representation of the nanoscratch experiment on **I**. b) and c) are the 2D and 3D piezo images of **I** after 300 μN load nanoscratch. d) Variation of lateral force along the scratch length at different loads on **I**. e) Friction coefficient plots at different scratch depths.

only at the surface of the crystal. No cracks due to experimental load were observed during scratch experiments.

Conclusions

This work probed the mechanical properties of dithiol protected Ag_{29} nanocrystals experimentally. Not only the observed Young's modulus and hardness values, 4.48 and 0.285 GPa, respectively, were similar to that of polymers, but the material also exhibited dynamic mechanical responses similar to polymeric materials. These experiments imply that the capping ligands play a significant role in the mechanical properties of nanocrystals. Moreover, this also indicates that such materials could be processed in very similar ways as polymers for device integration or could be easily incorporated into existing polymer-based devices to add extra functionality without any drastic changes in the mechanical properties of parent polymers. While these mechanical properties can be linked directly to the structure of the cluster and inter-cluster interactions in nanocrystals, unraveling those would require significant computational effort.

Experimental section

Chemicals: All chemicals, including sodium borohydride ($NaBH_4$, 99.99% metal basis), triphenylphosphine (TPP), benzene-1,3-dithiol (BDT) were purchased from Sigma-Aldrich. Silver nitrate ($AgNO_3$, 99%), was purchased from Rankem. Solvents including methanol, dichloromethane (DCM), dimethylformamide (DMF) were of HPLC grade.

Synthesis of $Ag_{29}(BDT)_{12}(TPP)_4$ nanoclusters: Synthesis of Ag_{29} nanoclusters (NCs) was performed by following a previously reported procedure.[18] Briefly, $Ag_{29}(BDT)_{12}$ NCs were prepared by dissolving 25 mg of silver nitrate in 5 mL of methanol. To this solution, 10 mL of DCM and 15 μL of BDT were added. After the addition of BDT, the solution changed to turbid yellow. The yellow colored solution became colorless by the addition of 200 mg of TPP (in 1 mL DCM). After 15 minutes, 10.5 mg of $NaBH_4$ in 500 μL deionized (DI) water was added. The color of the solution changed to dark brown after the addition of $NaBH_4$. After three hours of continuous stirring, the dark brown solution turned to orange. The orange solution was centrifuged and the supernatant was discarded. The residue was washed several times with methanol to remove excess thiols and thiolates and it was dispersed in DMF.

Crystallization of $Ag_{29}(BDT)_{12}(TPP)_4$ nanoclusters: The purified clusters were dispersed in DMF, and filtered using a syringe filter. The concentrated cluster solution was drop-casted on a microscope slide and kept undisturbed at room temperature. After 3–4 days luminescent red crystals were observed.

Characterization

UV-vis measurements: The absorption spectrum of the cluster solution was measured with a Perkin-Elmer Lambda 25 UV-vis absorption spectrophotometer. Spectrum was measured in the range of 190–1100 nm. The cluster was dissolved in the respective solvents and the spectrum was recorded in quartz cuvettes with 10 mm path length.

Luminescence measurements: Luminescence measurements of solution were carried out using the HORIBA JOBIN VYON NanoLog instrument. The bandpass for excitation and emission was set at 3 nm. Diluted cluster solution was used for the measurement. Emission spectra of the nanocrystals, especially from the indentation spots were collected on a confocal Raman microscope, Alpha 300 S from WiTec GmbH, using a 633-nm laser and 150 g/mm grating.

ESI-MS measurement: Waters Synapt G2-Si High Definition mass spectrometer equipped with electrospray ionization, matrix-assisted laser desorption ionization and ion mobility separation was used. The sample was analyzed in the negative mode of electrospray ionization. The instrument was calibrated using CsI as the calibrant.

SEM and EDAX measurements: Scanning electron microscopy (SEM) and energy dispersive X-ray (EDAX) analysis were done using an FEI QUANTA-200 SEM.

Nanoindentation measurements: Nanoindentation (NI) experiments were conducted using a Hysitron TI Premier nanomechanical testing instrument. For measuring mechanical properties, a three-sided Berkovich indenter, of radius 150 nm was used. The indentation loads ranged from 50 μN to 10,000 μN and a trapezoidal load function was used, which includes three segments. In the first segment, the load was increased linearly to its maximum in 20 s, the second segment corresponds to a constant holding of 10 s and in the third segment, the load was linearly decreased to zero in 10 s. In-situ SPM was used to examine the surface topographies prior to and after indentation. The E_r and H were calculated by applying the Oliver and Pharr method.[32] According to this method, E_r and H were determined from the initial part of the unloading segment of the load-displacement curve.

Nano DMA measurements: DMA was performed by using load controlled frequency sweep mode of nano-DMA. In this mode, the oscillating dynamic load was superimposed on static load over a frequency range of 10–200 Hz. The applied static load for all the samples was 200 μN and the dynamic load was 10 μN. The tests were carried out using a Berkovich indenter. A time-dependent nanomechanical property was analyzed by applying a sinusoidal force signal and capturing the displacement response at the same applied frequency by the nanoindentation system. The resulting phase lag from applied and resultant signal will provide information about the storage and loss moduli.

Nanoscratch measurements: Nano-scratch measurements were conducted using the Berkovich probe. In this technique, a 5 μM long scratch was made with three different loads (100, 200 and 300 μN) on three different crystals. The image was taken after each scratch through the in-situ SPM imaging technique to analyze the scratch response of the nanocrystal. The lateral force experienced by the probe was recorded as a function of displacement.

Supporting Information

Supporting Information is available from the Wiley Online Library or from the author.

Acknowledgements

We thank the Department of Science and Technology, Government of India for constantly supporting our research program

on nanomaterials. K.S.S. thanks the University Grants Commission (UGC), Govt. of India for a research fellowship. She also thanks, Sowmiya Narayani, Jyoti Sarita Mohanty and Papri Chakraborty for their help and suggestions.

Conflict of Interest

The authors declare no conflict of interest.

Keywords: cluster compounds · mechanical properties · nanoindentation · nanocrystals · single crystals

[1] a) W. Kurashige, Y. Niihori, S. Sharma, Y. Negishi, *Coord. Chem. Rev.* **2016**, *320*, 238–250; b) R. Jin, *Nanoscale* **2015**, *7*, 1549–1565; c) I. Chakraborty, T. Pradeep, *Chem. Rev.* **2017**, *117*, 8208–8271; d) P. D. Jadzinsky, G. Calero, C. J. Ackerson, D. A. Bushnell, R. D. Kornberg, *Science* **2007**, *318*, 430–433; e) H. Yang, Y. Wang, H. Huang, L. Gell, L. Lehtovaara, S. Malola, H. Häkkinen, N. Zheng, *Nat. Commun.* **2013**, *4*, 2422.
[2] A. Ghosh, V. Jeseentharani, M. A. Ganayee, R. G. Hemalatha, K. Chaudhari, C. Vijayan, T. Pradeep, *Anal. Chem.* **2014**, *86*, 10996–11001.
[3] a) Y.-S. Chen, H. Choi, P. V. Kamat, *J. Am. Chem. Soc.* **2013**, *135*, 8822–8825; b) V. Jeseentharani, N. Pugazhenthiran, A. Mathew, I. Chakraborty, A. Baksi, J. Ghosh, M. Jash, G. S. Anjusree, T. G. Deepak, A. S. Nair, T. Pradeep, *ChemistrySelect* **2017**, *2*, 1454–1463.
[4] S. Zhao, R. Jin, Y. Song, H. Zhang, S. D. House, J. C. Yang, R. Jin, *Small*, 1701519-n/a.
[5] G. Soldan, M. A. Aljuhani, M. S. Bootharaju, L. G. AbdulHalim, M. R. Parida, A.-H. Emwas, O. F. Mohammed, O. M. Bakr, *Angew. Chem. Int. Ed.* **2016**, *55*, 5749–5753.
[6] S. Chen, S. Wang, J. Zhong, Y. Song, J. Zhang, H. Sheng, Y. Pei, M. Zhu, *Angew. Chem. Int. Ed.* **2015**, *54*, 3145–3149.
[7] C. Zeng, C. Liu, Y. Chen, N. L. Rosi, R. Jin, *J. Am. Chem. Soc.* **2014**, *136*, 11922–11925.
[8] A. Das, T. Li, K. Nobusada, C. Zeng, N. L. Rosi, R. Jin, *J. Am. Chem. Soc.* **2013**, *135*, 18264–18267.
[9] D. Crasto, G. Barcaro, M. Stener, L. Sementa, A. Fortunelli, A. Dass, *J. Am. Chem. Soc.* **2014**, *136*, 14933–14940.
[10] M. W. Heaven, A. Dass, P. S. White, K. M. Holt, R. W. Murray, *J. Am. Chem. Soc.* **2008**, *130*, 3754–3755.
[11] C. Zeng, T. Li, A. Das, N. L. Rosi, R. Jin, *J. Am. Chem. Soc.* **2013**, *135*, 10011–10013.
[12] D. Crasto, S. Malola, G. Brosofsky, A. Dass, H. Häkkinen, *J. Am. Chem. Soc.* **2014**, *136*, 5000–5005.
[13] C. Zeng, H. Qian, T. Li, G. Li, N. L. Rosi, B. Yoon, R. N. Barnett, R. L. Whetten, U. Landman, R. Jin, *Angew. Chem. Int. Ed.* **2012**, *51*, 13114–13118.
[14] H. Qian, W. T. Eckenhoff, Y. Zhu, T. Pintauer, R. Jin, *J. Am. Chem. Soc.* **2010**, *132*, 8280–8281.
[15] A. Dass, S. Theivendran, P. R. Nimmala, C. Kumara, V. R. Jupally, A. Fortunelli, L. Sementa, G. Barcaro, X. Zuo, B. C. Noll, *J. Am. Chem. Soc.* **2015**, *137*, 4610–4613.
[16] H. Yang, J. Lei, B. Wu, Y. Wang, M. Zhou, A. Xia, L. Zheng, N. Zheng, *Chem. Commun.* **2013**, *49*, 300–302.
[17] C. P. Joshi, M. S. Bootharaju, M. J. Alhilaly, O. M. Bakr, *J. Am. Chem. Soc.* **2015**, *137*, 11578–11581.
[18] L. G. AbdulHalim, M. S. Bootharaju, Q. Tang, S. Del Gobbo, R. G. AbdulHalim, M. Eddaoudi, D.-e. Jiang, O. M. Bakr, *J. Am. Chem. Soc.* **2015**, *137*, 11970–11975.
[19] M. J. Alhilaly, M. S. Bootharaju, C. P. Joshi, T. M. Besong, A.-H. Emwas, R. Juarez-Mosqueda, S. Kaappa, S. Malola, K. Adil, A. Shkurenko, H. Häkkinen, M. Eddaoudi, O. M. Bakr, *J. Am. Chem. Soc.* **2016**, *138*, 14727–14732.
[20] a) C. Zeng, Y. Chen, K. Kirschbaum, K. J. Lambright, R. Jin, *Science* **2016**, *354*, 1580–1584; b) B. Yoon, W. D. Luedtke, R. N. Barnett, J. Gao, A. Desireddy, B. E. Conn, T. Bigioni, U. Landman, *Nat. Mater.* **2014**, *13*, 807–811.
[21] S. Varughese, M. S. R. N. Kiran, U. Ramamurty, G. R. Desiraju, *Angew. Chem. Int. Ed.* **2013**, *52*, 2701–2712.
[22] C. Sun, D. J. W. Grant, *Pharm. Res.* **2001**, *18*, 274–280.
[23] A. Richter, R. Ries, R. Smith, M. Henkel, B. Wolf, *Diamond Relat. Mater.* **2000**, *9*, 170–184.
[24] a) M. R. VanLandingham, *J. Res. Natl. Inst. Stand. Technol* **2003**, *108*, 249–265; b) J. L. Loubet, J. M. Georges, O. Marchesini, G. Meille, *J. Tribol.* **1984**, *106*, 43–48.
[25] J. C. Tan, J. D. Furman, A. K. Cheetham, *J. Am. Chem. Soc.* **2009**, *131*, 14252–14254.
[26] a) K. Kimura, T. Pradeep, *Phys. Chem. Chem. Phys.* **2011**, *13*, 19214–19225; b) K. E. Mueggenburg, X.-M. Lin, R. H. Goldsmith, H. M. Jaeger, *Nat. Mater.* **2007**, *6*, 656; c) P. Podsiadlo, G. Krylova, B. Lee, K. Critchley, D. J. Gosztola, D. V. Talapin, P. D. Ashby, E. V. Shevchenko, *J. Am. Chem. Soc.* **2010**, *132*, 8953–8960.
[27] W. Cheng, M. J. Campolongo, J. J. Cha, S. J. Tan, C. C. Umbach, D. A. Muller, D. Luo, *Nat. Mater.* **2009**, *8*, 519.
[28] U. Landman, W. D. Luedtke, *Faraday Discuss.* **2004**, *125*, 1–22; discussion 99–116.
[29] E. Tam, P. Podsiadlo, E. Shevchenko, D. F. Ogletree, M.-P. Delplancke-Ogletree, P. D. Ashby, *Nano Lett.* **2010**, *10*, 2363–2367.
[30] A. Ghosh, D. Ghosh, E. Khatun, P. Chakraborty, T. Pradeep, *Nanoscale* **2017**, *9*, 1068–1077.
[31] a) G. H. Ahmed, M. R. Parida, A. Tosato, L. G. AbdulHalim, A. Usman, Q. A. Alsulami, B. Murali, E. Alarousu, O. M. Bakr, O. F. Mohammed, *J. Mater. Chem. C* **2016**, *4*, 2894–2900; b) S. M. Aly, L. G. AbdulHalim, T. M. D. Besong, G. Soldan, O. M. Bakr, O. F. Mohammed, *Nanoscale* **2016**, *8*, 5412–5416.
[32] W. C. Oliver, G. M. Pharr, *J. Mater. Res.* **2011**, *7*, 1564–1583.
[33] a) D. Ciprari, K. Jacob, R. Tannenbaum, *Macromolecules* **2006**, *39*, 6565–6573; b) K. Komvopoulos, L. Pruitt, C. Klapperich, *J. Tribol.* **2001**, *123*, 624–631; c) G. Mallikarjunachari, P. Ghosh, *Polymer* **2016**, *90*, 53–66.
[34] X. W. Gu, X. Ye, D. M. Koshy, S. Vachhani, P. Hosemann, A. P. Alivisatos, *Proc. Natl. Acad. Sci. U.S.A.* **2017**, *114*, 2836–2841.
[35] A. Zandiatashbar, C. R. Picu, N. Koratkar, *Small* **2012**, *8*, 1675–1675.
[36] W. Paul, D. Oliver, P. Grutter, *Phys. Chem. Chem. Phys.* **2014**, *16*, 8201–8222.
[37] L. Ugarte, S. Gómez-Fernández, C. Peña-Rodríuez, A. Prociak, M. A. Corcuera, A. Eceiza, *ACS Sustainable Chem. Eng.* **2015**, *3*, 3382–3387.

Manuscript received: December 5, 2017
Version of record online: ■■, ■■■

FULL PAPER

Light mechanics: The mechanical properties of luminescent single crystals of atomically precise clusters were investigated. The observed Young's modulus of the crystals was similar to that of hard polymers, which reveals the key role played by the protecting ligands in deciding the mechanical properties. No fracture was observed when a higher load of 10,000 μN was applied on the single crystals.

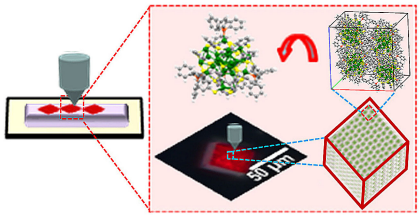

Cluster Crystals

K. S. Sugi, G. Mallikarjunachari, A. Som, Prof. P. Ghosh, Prof. T. Pradeep**